

LA-UR-09-01090

Approved for public release;
distribution is unlimited.

<i>Title:</i>	Report on AES 003 1.3 GHz 9-cell Superconducting Niobium Cavity Test Results At LANL
<i>Author(s):</i>	G. Ereameev , A. Canabal, T. Tajima, A. Bhatti, F. Krawczyk, R. Roybal
<i>Intended for:</i>	Distribution.



Los Alamos National Laboratory, an affirmative action/equal opportunity employer, is operated by the Los Alamos National Security, LLC for the National Nuclear Security Administration of the U.S. Department of Energy under contract DE-AC52-06NA25396. By acceptance of this article, the publisher recognizes that the U.S. Government retains a nonexclusive, royalty-free license to publish or reproduce the published form of this contribution, or to allow others to do so, for U.S. Government purposes. Los Alamos National Laboratory requests that the publisher identify this article as work performed under the auspices of the U.S. Department of Energy. Los Alamos National Laboratory strongly supports academic freedom and a researcher's right to publish; as an institution, however, the Laboratory does not endorse the viewpoint of a publication or guarantee its technical correctness.

Report on AES 003 1.3 GHz 9-cell Superconducting Niobium Cavity Test Results at LANL*

G. Ereemeev[†], A. Canabal, T. Tajima, A. Bhatti, F. Krawczyk, R. Roybal
LANL, Los Alamos, NM 87544, USA

Abstract

A superconducting niobium 9-cell 1.3 GHz cavity, AES #003, was tested at LANL using recently developed full temperature mapping system and surface inspection system. The cavity was limited by field emission in the π mode as was indicated by radiation detectors and the characteristic pattern on the temperature map. The 9-cell thermometry system also identified excess heating in other areas. Following the test the cavity was disassembled from the vertical test stand, and the inside was inspected with the recently built surface inspection system. During inspection defects on the cavity surface were found where excess heating was shown by the 9-cell thermometry system.

INTRODUCTION

For the ILC main linac about 16000 9-cell superconducting RF cavities are required to achieve 35 MV/m accelerating gradient in a vertical test and to operate at the average gradient of 31.5 MV/m in a horizontal cryomodule, and another 1200 9-cell cavities will provide acceleration in the sources and bunch compressors [1]. Today, the leading manufacturer of high-performance 9-cell superconducting cavities is ACCEL, but, in order to have capability to split the production load among several manufacturers, a few companies in the North American region are being supported to produce high-quality superconducting niobium cavities. These companies are still working on refining their processes. Among these companies are Advanced Energy Systems, Niowave, Roark and Pavak. The most experienced at the moment is Advanced Energy Systems, which has already produced several 9-cell cavities. Still, most of these cavities were limited to about 25 MV/m in vertical tests. Therefore, further development in the production process is required to meet ILC specifications.

In order to improve the performance, it is necessary to identify the source of degradation. For such identification a 9-cell thermometry system coupled with an inside-surface inspection system is the best tool. The high cost of such tool is an obstacle, but it has been recently overcome at LANL. A new 9-cell thermometry system was designed and built at LANL [2], along with a new surface inspection system [3]. As part of these 9-cell thermometry and inspection systems' evaluation we measured RF properties of an AES cavity, AES #003, with RF setup and recorded heating areas in different modes with the new 9-cell thermometry system. After the RF test the cavity was moved

to the cleanroom and the inside surface of the cavity was inspected with the new surface inspection system.

CAVITY HISTORY

The cavity, manufactured by AES [4], after fabrication was tested at TJNAF, where it underwent a number of preparation steps:

- 150 μm EP
- Degreasing
- 20 μm EP
- Degreasing
- First HPR
- Drying in the cleanroom
- First cleanroom assembly
- Second HPR + drying
- Final cleanroom assembly
- Pumping down and leak check
- Low temperature baking at 110 °C

After the low temperature baking the cavity was tested at 2 °K. The cavity was found to be limited by a quench either in the 4th or 6th cell at about $E_{acc}=20$ MV/m, as determined by the pass-band modes measurement. To increase the quench field, the cavity was electropolished for another 200 μm . After preparation similar to that prior to the first test, the cavity was RF tested again. In the second test the cavity was still limited by the quench. After the second test the cavity was shipped to Fermilab, where it was tested several times. In the first test the cavity was again limited at 20 MV/m by the quench. After the first test at Fermilab a variable coupler was installed for the next test. In the next test the cavity was limited by the field emission at about 10 MV/m. It was speculated that field emission was introduced during installation of the variable coupler. The variable coupler was replaced with the fixed coupler, but in the subsequent tests the cavity was still limited by the field emission at about 10 MV/m. After testing the cavity was shipped to LANL for testing with the thermometry system. At LANL the cavity was high-pressure rinsed with ultra-pure water. Following rinsing the cavity was left drying in the cleanroom class 100. Next, the cavity was removed from the high-pressure-rinsing system, and, the input coupler was assembled onto the cavity in the cleanroom class 100. After assembly the cavity was taken out of the cleanroom, and assembled on the test stand. The cavity then was pumped down, and, later, baked at 100 °C for 48 hours. After baking the 9-cell thermometry system was assembled to the cavity, and the cavity was inserted into cryostat for testing at 2 °K.

* This work was supported by DOE

[†] grigory@lanl.gov

TEST RESULTS

RF results

The quality factor of the cavity at 2 °K as a function of field in the π mode is presented in Fig. 1. The highest field was limited by the available power. X-ray radiation up to 8 R/h was registered at the highest field in the π mode by the X-ray sensor at the top lid of the cryostat. A quality factor close to 10^{10} was measured at low fields, but it had strong field dependence due to field emission, dropping to $3 \cdot 10^9$ at $E_{acc} \cong 8$ MV/m.

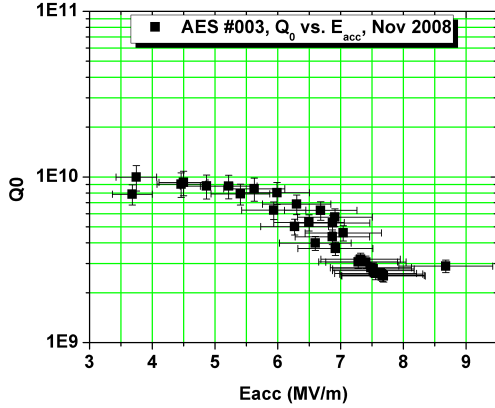


Figure 1: The quality factor of AES 003 as a function of field gradient in the π mode. The highest field was limited by available power (200W at the output of amplifier). The quality factor degradation is due to the field emission. Error bars were calculated from the variation in the calibration data measured at several points.

In order to avoid the field emission problem the cavity was tuned to other modes. For reference, in Fig. 2 the field distribution for each modes is presented. The summary of results in other modes is presented in Table. 1. Notably, X-rays were detected also in the $6\pi/9$ mode.

Table 1: The frequencies of different modes with the highest transmitted power for a given mode and corresponding field in end-cells.

mode	F Hz	max Pt mW	end cell Eacc MV/m
$\pi/9$	1.27525E9	2.179	2.9
$2\pi/9$	1.27765E9	3.2	3.5
$3\pi/9$	1.28083E9		--
$4\pi/9$	1.28507E9	10.8	6.4
$5\pi/9$	1.28938E9	12.25	6.8
$6\pi/9$	1.2936E9	43	12.7
$7\pi/9$	1.29725E9	24	9.5
$8\pi/9$	1.29946E9	20.5	8.8
π	1.30028E9	20.1	8.7

The highest transmitted power in each mode gives the accelerating gradient in end-cells. Knowing the accelerating gradient and field distribution in different modes, we calculated highest accelerating gradient, see Table. 2, for

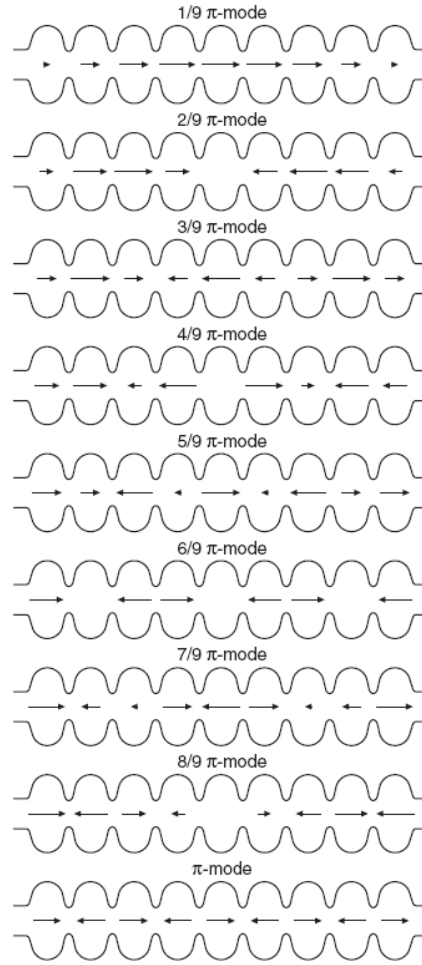


Figure 2: The field distribution in the cavity for different modes [5].

Table 2: The highest achieved accelerating gradients in MV/m for each cell, as calculated from the field profiles in different modes.

cell#	max. Eacc MV/m
1	12.9
2	8.8
3	12.6
4	15.4
5	16.4
6	15.4
7	12.6
8	8.8
9	12.9

each cell. The highest accelerating gradient, $E_{acc} \cong 16$ MV/m was reached in the center cell.

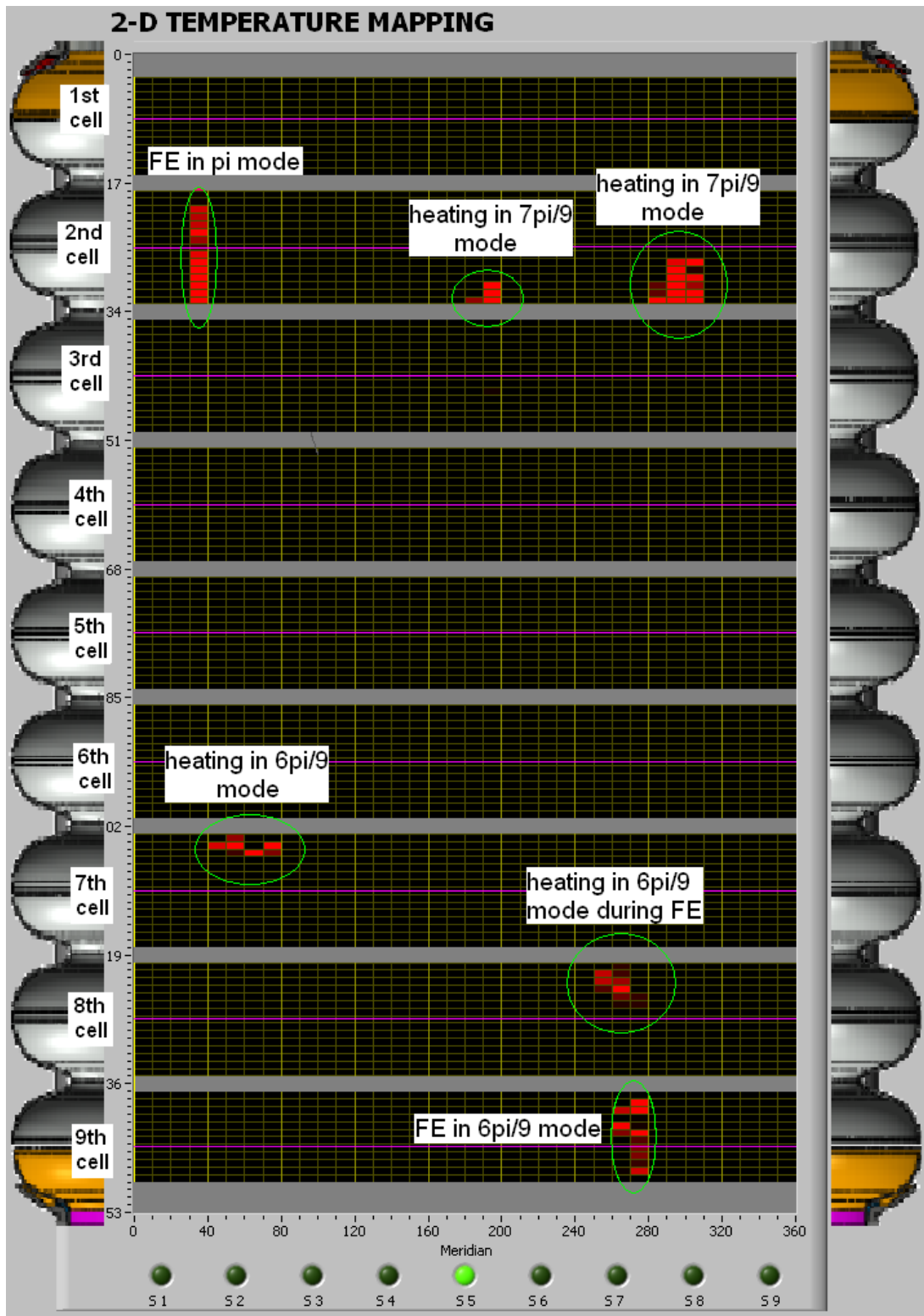


Figure 3: Summary of defects found on the cavity surface. The temperature scale and field scale are different for different hot-spots, so this picture only illustrates positions of different defects. The regions near cavity irises, where temperature sensors were not placed due to the interference with stiffening rings or disks at the end cells, were grayed out on the temperature map. For reference the cavity drawing is presented. Thermometers on equators are marked with magnets.

Thermometry results

The cells were numbered from pickup coupler side. For the azimuthal direction, the center of HOM coupler on the pickup coupler side was set to 0 degree and the angle was shown clockwise looking the cavity from the pickup coupler side. For reference we put all heating areas found with thermometry system on the same temperature map, Fig. 3. Because these hot-spots were measured in different modes, at different field levels, they are not to be compared directly, they are presented only for a quick reference. All original temperature maps are presented in the Appendix. In the π mode the dominant source of losses was field emission in the 2nd cell. The temperature map clearly shows pattern, characteristic for field emission, see Fig. 15 in the Appendix. The field emission in the $6\pi/9$ mode was shown to be located in the 9th cell, see Fig. 14 in the Appendix. Heating was also observed in 8th cell, which has zero field in this mode. It is speculated that some electrons produced during field emission in the 9th cell, travelled to the 8th cell and deposited their energy there. Also, in the $6\pi/9$ mode distributed heating was observed in the 7th cell near the top iris, Fig. 13 in the Appendix. In the $7\pi/9$ mode two more heating areas were found by thermometry system in the 2nd cell, Fig. 11 and Fig. 12 in the Appendix. In other modes the highest achieved field was determined by available power without any heating registered by the thermometry system. It should be noted that the sensitivity of the thermometry was reduced by parasitic 60 Hz noise, present in the thermometry system throughout the tests.

INSPECTION RESULTS



Figure 4: The top HOM coupler was used as a reference point to mark the position of the board zero of the thermometry system. Thermometry boards were placed every ten degrees in ascending order clockwise around the cavity as viewed from the top. For more information on the thermometry system, please, refer to [2].

After the test the cavity was taken out from the cryostat. The thermometry system was disassembled, and the suspected lossy regions were marked, e.g. Fig. 5. After the cavity was degassed, removed from the test stand and

moved to the cleanroom class 100. In the cleanroom the cavity was cleaned with methanol and filled with N₂ gas slowly overnight. After slightly pressurizing the cavity to avoid an inadvertent particle contamination of the cavity, the input coupler was disassembled from the cavity, and the cavity was put on the inspection system for the surface inspection. The whole surface of the cavity was inspected with particular attention to the areas, noted by the thermometry system as lossy.



Figure 5: The position of the board, where field emission was observed, was marked after removing the thermometry system. These areas were closely examined during the surface inspection.

Please note that the distance markers added to some of the inspection results might not be accurate since we used a distance measurement function that came with the videoscope and has not been calibrated.

In the 2nd cell, near the iris between the 2nd and 3rd cells, we observed a pit in the stiffening ring weld, Fig. 6. We suspect this weld defect as a possible cause for field emission in the π mode.



Figure 6: The picture of the inside surface, where field emission heating was identified with the thermometry system. A defect, which is suspected to be the cause of field emission, was found on the stiffening ring weld, at the bottom of the cell, near the iris between the 2nd and 3rd cells, at 30 degrees.

Another two hot-spots were indicated in the 2nd cell by

the thermometry system. They are marked as "heating in $7\pi/9$ mode" in Fig. 3. Inspecting the cavity, we found two surface defects about 1-2 mm from each other, Fig. 7, at about 190° at the bottom iris of the 2^{nd} cell, where the 9-cell thermometry system indicated excess heating during the RF test. No visible defects were found during examination of the 2^{nd} -cell's bottom iris at 280 - 300° , where the thermometry system also indicated a hot-spot. Here, however, the broad area of heating suggests a defect other than a small pit or a foreign inclusion on the niobium surface.



Figure 7: The picture of the inside surface on the bottom of the cell, near the iris between the 2^{nd} and 3^{rd} cells, at 190 degrees, where a defect heating was identified with the thermometry system. A defect found here on the inside surface is suspected to be the cause of heating.

In the 6^{th} cell, near the top iris, another area was found to have higher losses as shown by the thermometry system, Fig. 3. During the surface inspection of the cavity we found two scratches at the iris between the 5^{th} and 6^{th} cell, Fig. 8, exactly at the location, where the thermometry indicated higher losses.



Figure 8: The picture of the inside surface of the iris between the 6^{th} and 7^{th} cells, at 70 degrees, where a defect heating was identified with the thermometry system. Two scratches on the surface are suspected to be the cause of excess dissipation.

Another source of heating in the $6\pi/7$ mode was located

in the 9^{th} cell as was registered by the thermometry system. During visual inspection of that area we found a defect on the cavity surface, Fig. 9



Figure 9: The picture of the inside surface of the 9^{th} cell's bottom, at 260 degrees, where field emission was identified with the thermometry system. The defect found near the iris of the 9^{th} cell is suspected to be the cause of field emission.

We also would like to note that during surface inspection a number of pits were found on the surface, Fig. 10. Though no excess of heating was measured near those defects with the thermometry system, these defect may cause a premature thermal breakdown at fields higher than those reached in the recent test.



Figure 10: The picture of the inside surface near the top iris of the 5^{th} cell, at 180 degrees, where no excess of dissipation was present on the temperature maps during the test. Yet, defects found here, and those found in other areas of the cavity present a potential problem for achieving high field.

CONCLUSION

We have successfully tested a 9-cell 1.3 GHz cavity with recently developed full thermometry system and surface inspection system. The limitation in the π mode was a severe field emission, as was found with our new 9-cell thermometry system. Several other lossy areas were identified by

the thermometry system. After the test the cavity was inspected with the new surface inspection system. Surface defects were found in areas that were lossy, as detected with the 9-cell thermometry system. A significant number of pit-like defects found on the cavity surface suggest a poor quality of niobium material, which must be improved if high gradients are to be achieved.

ACKNOWLEDGEMENT

This work was initially funded by DOE office of Science Office of High Energy Physics in 2007. Since May 2008 Defense Threat Reduction Agency (DTRA) has funded us to complete the full temperature mapping and surface inspection systems. The authors would like to thank them for their support.

We also would like to thank Shekar Mishra, Mark Champion, Camille Ginsburg, Tug Arkan et al. of FNAL for loaning us a cavity for commissioning the temperature mapping and surface inspection systems. We also acknowledge the help of Gigi Ciovati and Rongli Geng of JLab for some initial Allen-Bradley resistor measurements and providing us with passband modes data, respectively, as well as Zach Conway of Cornell University for giving us info on the field patterns for each mode.

Finally, we would like to thank our LANL colleagues John Chamberlin, John Harrison and Felix Olivas for some assemblies and James Sedillo for LabView temperature map program.

REFERENCES

- [1] N. Phinney, N. Toge, and N. Walker, eds., "International Linear Collider Reference Design Report, Volume 3: Accelerator", p. 157 (2007).
- [2] A. Canabal et al., to be published.
- [3] T. Tajima et al., to be published.
- [4] C. Ginsburg, "Overview of US work on AES", (2008).
- [5] E. Vogel, "High gain proportional rf control stability at TESLA cavities", Phys. Rev. ST AB 10, 052001 (2007).

APPENDIX

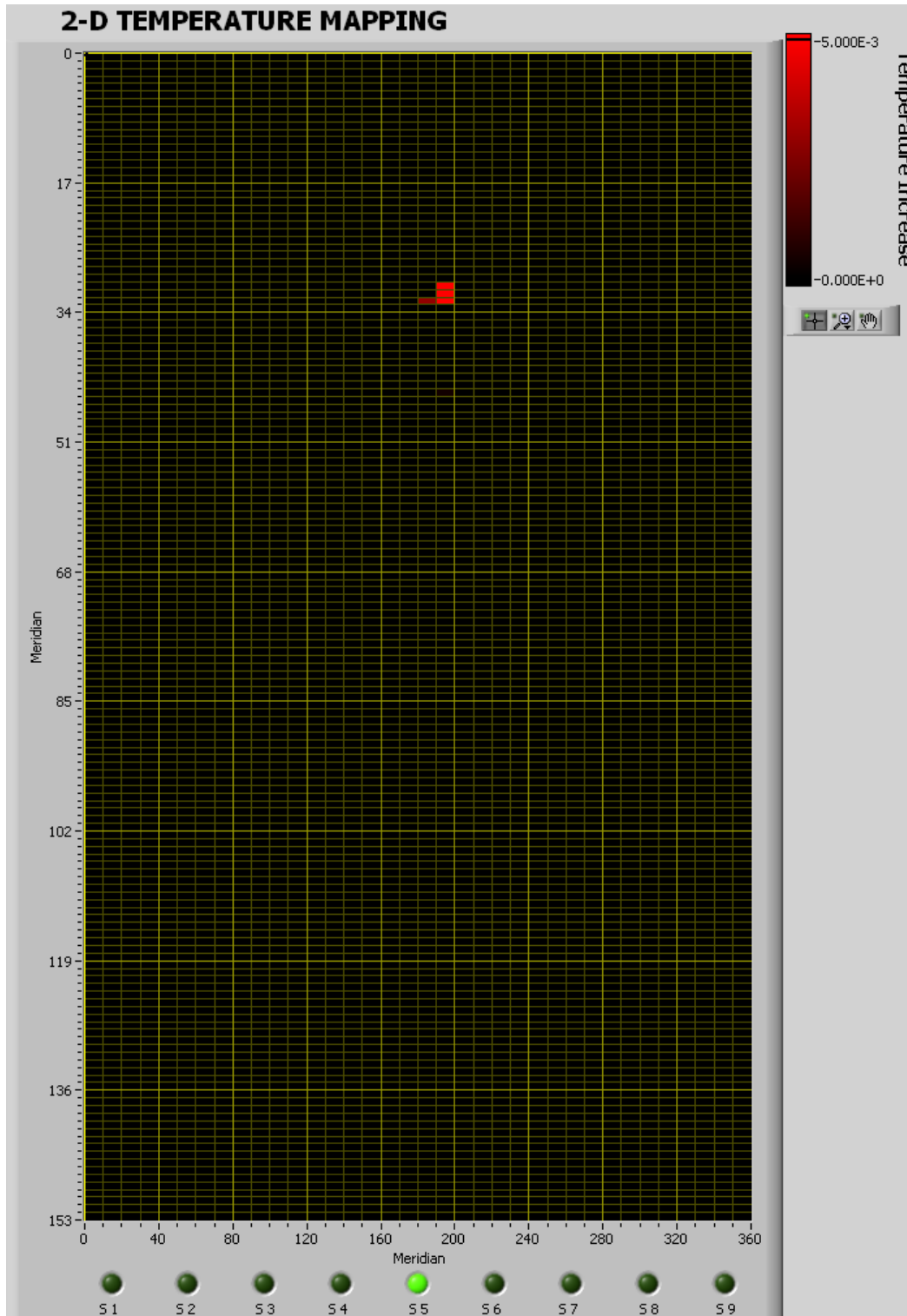


Figure 11: The temperature map saved during testing in the $7\pi/9$ mode shows defect heating in the 2nd cell.

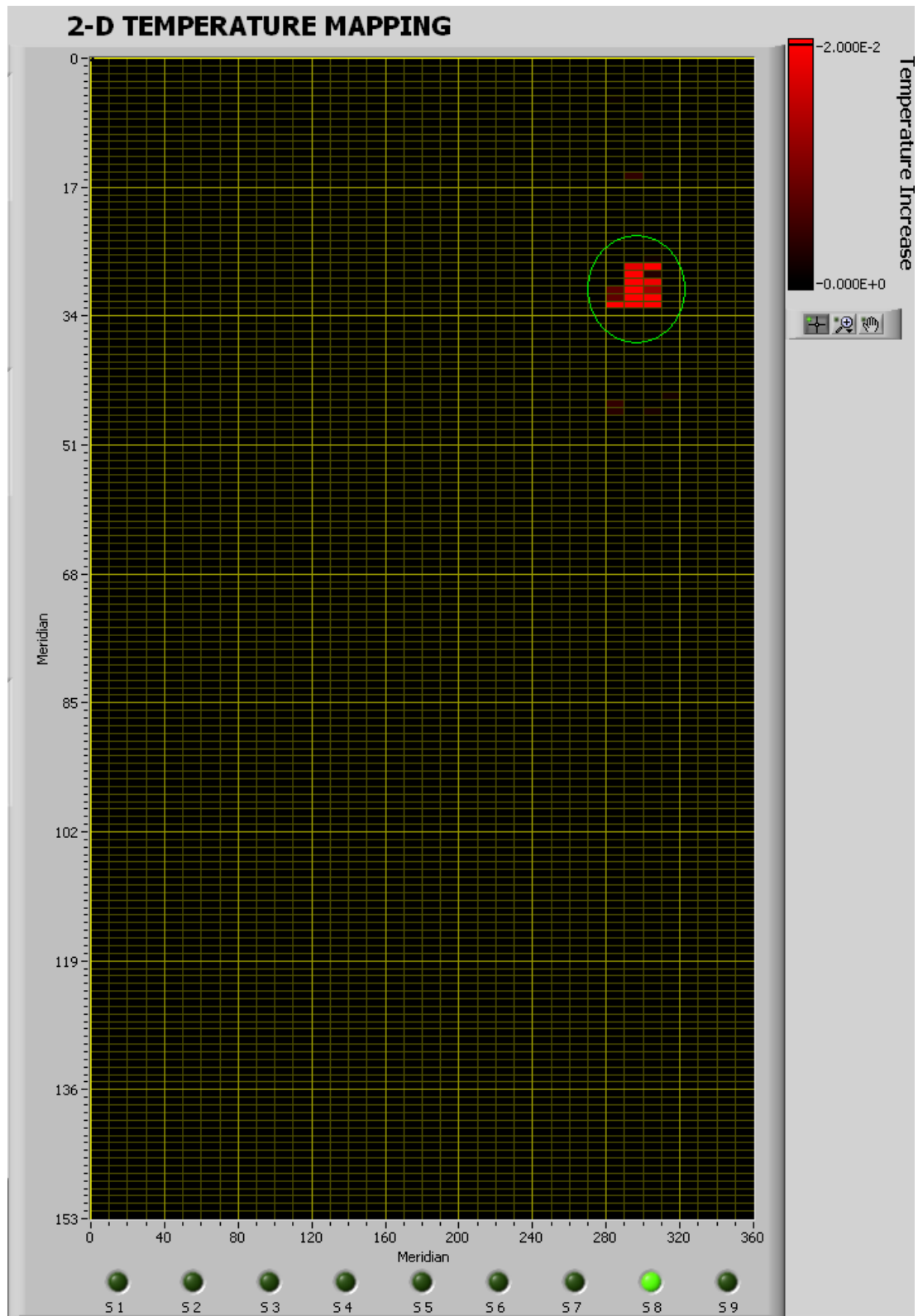


Figure 12: The temperature map saved during RF testing in the $7\pi/9$ mode shows excess heating in the 2^{nd} cell.

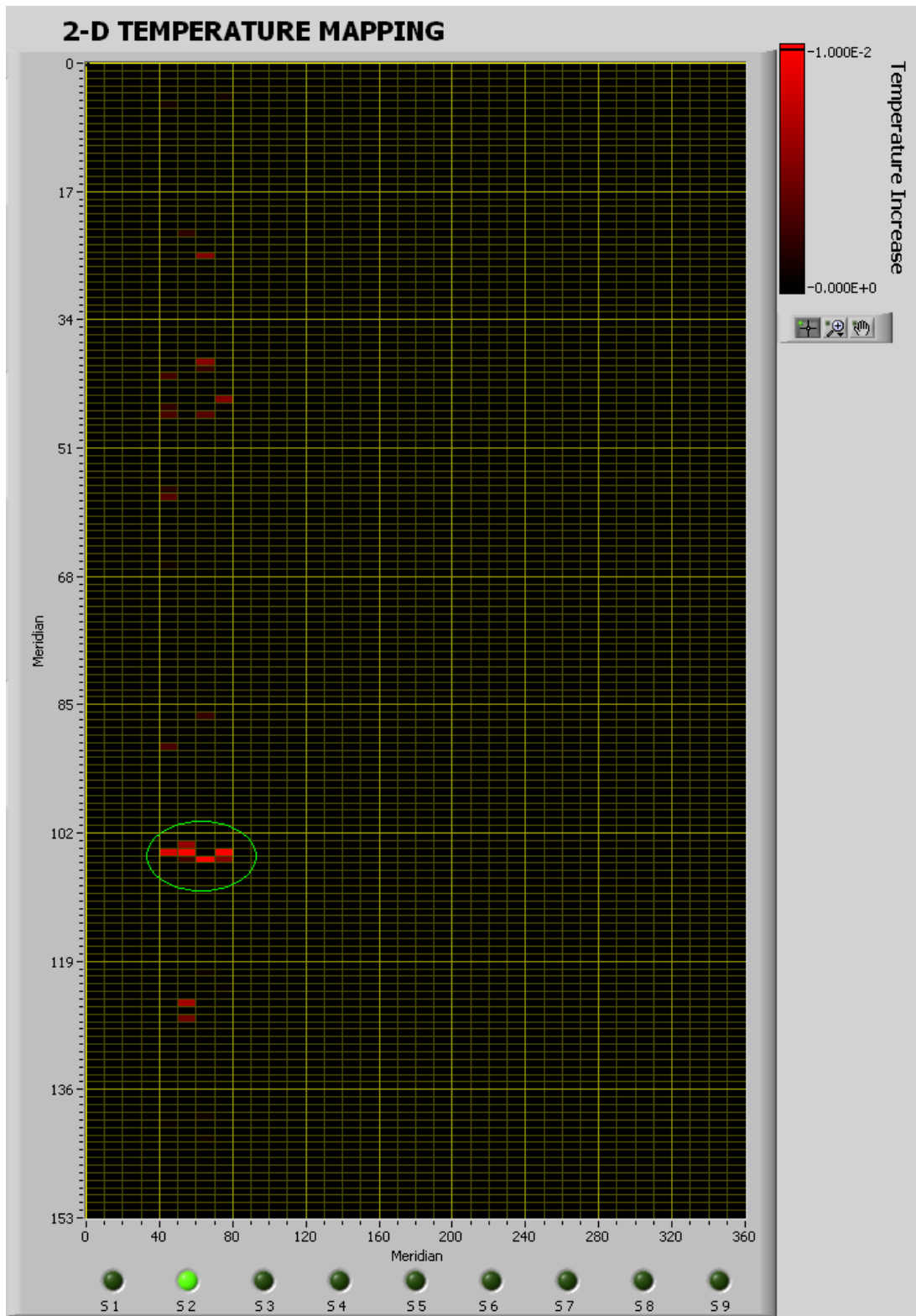


Figure 13: The temperature map saved during RF testing in the $6\pi/9$ mode shows excess heating in the 7th cell.

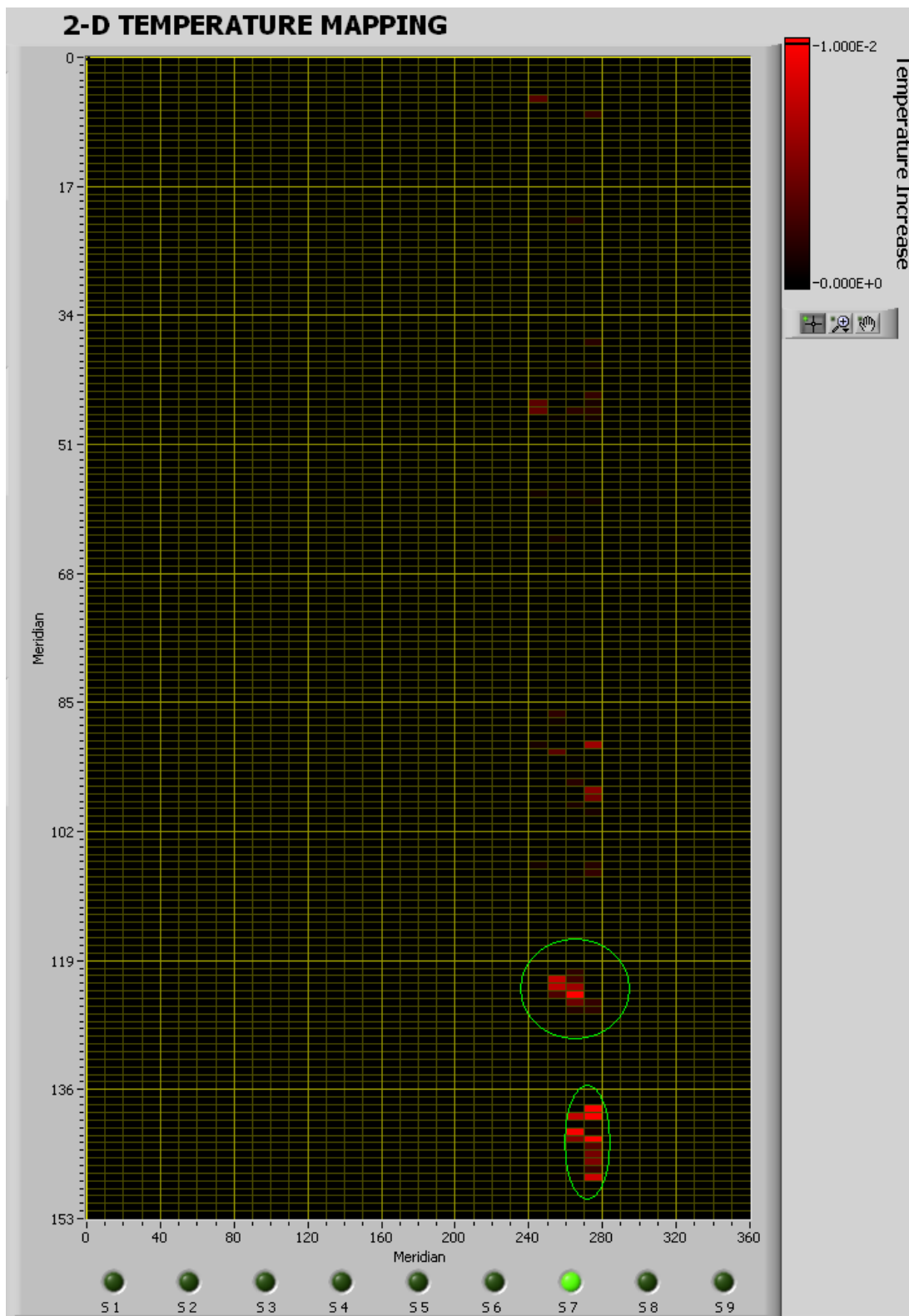


Figure 14: The temperature map saved during RF testing in the $6\pi/9$ mode shows excess heating in the 9th cell.

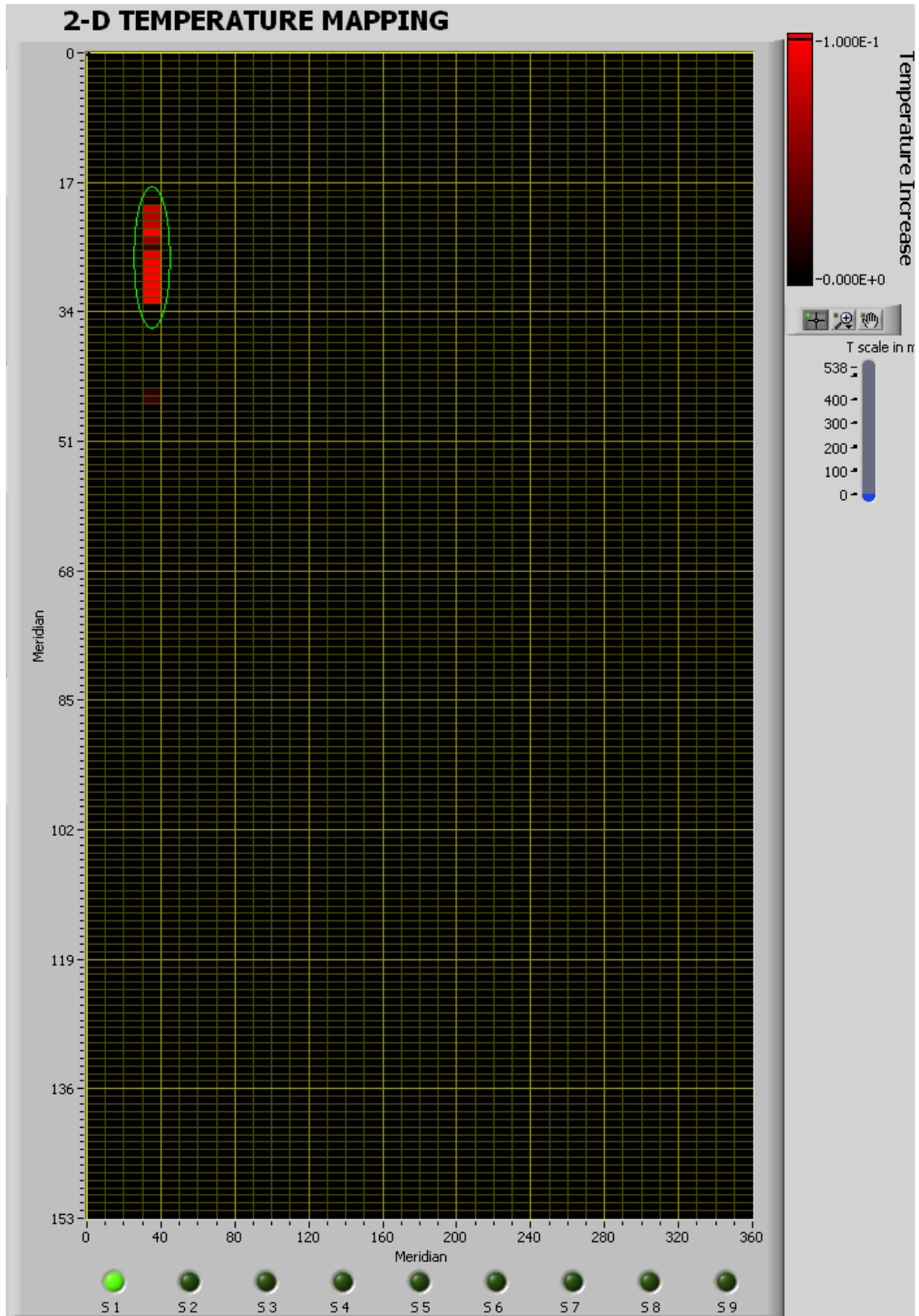


Figure 15: The temperature map saved during RF testing in the π mode shows field emission heating in the 2th cell. This heating was the ultimate limitation in RF performance of the cavity in the π mode.